MODERN TECHNIQUES FOR CHARACTERIZING MAGNETIC MATERIALS

MODERN TECHNIQUES FOR CHARACTERIZING MAGNETIC MATERIALS

Edited by

YIMEI ZHU

KLUWER ACADEMIC PUBLISHERS
Boston / Dordrecht / London

Library of Congress Cataloging-in-Publication Data

A C.I.P. Catalogue record for this book is available
from the Library of Congress.

Modern techniques for characterizing magnetic materials / edited by Yimei Zhu.
p. cm
Includes bibliographical references and index.
ISBN 1-4020-8007-7 (alk, paper) -- ISBN 0-387-23395-4 (e-book)
1. Magnetic materials—Analysis. 2. Magnetic materials –Microscopy. 3. Electrons –
Scattering, I. Zhu, Yimei.

QC765.M63 2005
538'.4—dc22

2005042533

Printed in the United States of America. (BS/DH)

9 8 7 6 5 4 3 2 1 SPIN 11052838

springeronline.com

Authors

Rolf Allenspach
IBM Research
Rüschlikon, Switzerland

Ernst Bauer
Arizona State University
Arizona, USA

Marco Beleggia
Brookhaven National Laboratory
New York, USA

Matthias Bode
University of Hamburg
Hamburg, Germany

Byoung-Chul Choi
University of Victoria
British Columbia, Canada

Dan Dahlberg
University of Minnesota
Minnesota, USA

Michael Fitzsimmons
Los Alamos National Laboratory
New Mexico, USA

Mark Freeman
University of Alberta
Edmonton, Alberta, Canada

Paul Fumagalli
Free University of Berlin
Berlin, Germany

Daniel Haskel
Argonne National Laboratory
Illinois, USA

Burkard Hillebrands
Technical University of Kaiserslautern
Kaiserslautern, Germany

Joachim Kohlbrecher
Paul Scherrer Institute
Villigen, Switzerland

Jeffery B. Kortright
Lawrence Berkeley National Laboratory
California, USA

Alexander Krichevsky
Naval Research Laboratory
Washington, DC, USA

Andre Kubetzka
University of Hamburg
Hamburg, Germany

Jonathan C. Lang
Argonne National Laboratory
Illinois, USA

Seung-Hun Lee
National Institute of Standards and Technology
Maryland, USA

Charles F. Majkrzak
National Institute of Standards and Technology
Maryland, USA

Oswald Pietzsch
University of Hamburg
Hamburg, Germany

Roger Proksch
Asylum Research
California, USA

George Srajer
Argonne National Laboratory
Illinois, USA

Elio Vescovo
Brookhaven National Laboratory
New York, USA

Werner Wagner
Paul Scherrer Institute
Villigen, Switzerland

Roland Wiesendanger
University of Hamburg
Hamburg, Germany

Igor Zaliznyak
Brookhaven National Laboratory
New York, USA

Yimei Zhu
Brookhaven National Laboratory
New York, USA

Preface

Magnetism and magnetic phenomena surround us. Magnetic materials pervade our lives far beyond just compasses and common household magnets. Magnetic materials and magnetism are used inconspicuously in many complex gadgets, ranging from magnetic recording disks and cellular phones, to magnetic resonance imaging instruments and spintronic devices. Understanding magnetic phenomena and developing new functional magnetic materials pose a big challenge, but also great opportunities, to our scientists and engineers. New characterization techniques help us to understand the fascinating behavior of newly discovered magnetic materials, while new materials stimulate the further development of novel methods.

We understand the physical and chemical behaviors of materials through directly or indirectly measuring a material's structure and properties. The field of structural characterization is often too wide; identifying the most appropriate method to employ can be difficult. One objective of this book is to introduce the reader to various modern techniques in characterizing magnetic materials at different length scales, focusing on neutron, x-ray, electron, and laser-light scattering as well as proximal probes, their principles, applicability, limitations, and relationship to competing methods.

Neutrons, photons, and electrons are three major classes of modern probes for characterizing structures of materials. Since all materials absorb and emit electromagnetic radiation, the material's characteristics frequently manifest in the way it interacts with incident particles. Thus, the information gleaned not only depends on the wavelength of the radiation, but also on the nature of these interactions. Neutrons interact with atomic nuclei, x-ray photons with electron clouds, and electrons with electromagnetic potentials, i.e., both electrons and nuclei of the solid. For magnetic structural characterization, both electrons and nuclei in materials have a magnetic moment and, in principle, all the three sources can reveal magnetic information. In particular, because the neutron has spin ½, the orientation of its spin is easily manipulated and when combined with scattering geometry, it yields an opportunity to measure the spatial dependence of the vector magnetization. However, neutrons are not handily and copiously produced. In contrast, x-rays are easy to generate, but due to their weak spin interaction with matter, magnetic scattering can only be observed using extraordinarily intense synchrotron radiation.

The past two decades have witnessed significant advancement in instrumentation and technique development in characterization of magnetic materials, especially in proximal probes and laser-light scattering, along with the newly constructed next-generation neutron and synchrotron photon sources. In domain imaging, for example, an important branch of the field, we see an ever-increasing spatial resolution. There is a multiplicity of techniques, ranging from magneto-optical imaging to spin polarized scanning tunneling microscopy, that have different mechanisms of image formation and are suitable, hence, for different measurements. For instance, magneto-optic microscopy is based on the contrast produced by Kerr rotation of linearly polarized light reflected off domains with different magnetization. It has a typical spatial resolution of 500-1000nm (which can be much improved by near-field optical microscopy), but superior time resolution of up to 10-9 sec for dynamic observations. Magnetic force microscopy (MFM), on the other hand, measures the force that the stray magnetic field of the surface exerts on a tiny magnetic tip attached to a flexible cantilever. Unlike other methods, it is mainly sensitive to field gradients and its resolution is on the order of 40-100 nm. Scanning electron microscopy with

polarization analysis (SEMPA) measures the spin polarization of secondary electrons emitted from a magnetized sample with resolution of about 30-200 nm. Spin polarized low energy electron microscopy (SPLEEM) is a surface-imaging technique using spin polarized electrons, and is sensitive to the interaction between the spins of the incident electron and the spins in the sample. Thus, surface magnetic behavior can be directly observed over a large area of view in real time with a resolution of 20nm. High-energy transmission electron microscopy techniques push resolution even further. A remarkable example is electron holography which is based on retrieving the phase shift of a coherent electron wave passing though the sample as encoded in a hologram, and provides a direct measure of the electrostatic and magnetic potentials of a local area of interest. Although a few nm resolution can be routinely achieved, separating magnetostatic potentials from electrostatic ones at the nanoscale can be challenging. To date, the most promising technique for attaining atomic resolution of local magnetic structure is spin-polarized scanning tunneling microscopy (SP-STM) that can reveal the magnetic lattice arrangement on an antiferromagnetic sample surface. This new breed of scanning tunneling microscopy measures the spin-polarized tunneling electrons between the tip and the sample.

Of course, the techniques for magnetic imaging exemplified here are not meant to be inclusive, as several others are available, notably the recently developed technique of synchrotron-based x-ray magnetic microscopy, i.e., the x-ray magnetic circular dichroism (XMCD). This method probes the transfer of the angular momentum of the x-ray photon to the photoelectron excited from a spin-orbit split core level with a spatial resolution of about 5 nm. The main advantage of the technique is its elemental specificity that derives from the process being tied to an absorption event at the core level, thus providing information on the spin orbital moments, site symmetry, and chemical state of the sample under study, which is not available from the desktop- or laboratory-instruments mentioned earlier. It is important to realize that these techniques are complementary; they all have their own advantages and drawbacks. Some are highly penetrating and non-destructive probes, while others require a high-quality surface or tedious sample preparation. If you are interested in these technologies and would like to know more about them, you will find this book, Modern Techniques for Characterizing Magnetic Materials, an invaluable tool for expanding your research capabilities.

This book is organized in the following way. The first three chapters deal with neutron scattering methods, including triple-axis spectrometry, small-angle scattering, and reflectometry. Chapter 4-6 focus on synchrotron-radiation based techniques, ranging from magnetic soft and hard x-ray scattering to photon-emission spectroscopy. Chapter 7-9 discuss electron scattering, with transmission electron microscopy focusing on Lorentz microscopy, electron holography and other phase-retrieval methods, and scanning electron microscopy with spin polarized analysis and spin polarized low energy electron microscopy. Chapter 10 and 11 describe proximal probes, covering spin-polarized scanning tunneling microscopy and magnetic force microscopy. The last three chapters deal with light scattering including the use of monochromatic laser light in magnetic imaging, such as scanning near-field optical microscopy, time-resolved scanning Kerr microscopy, and Brillouin light-scattering spectroscopy.

This book does not attempt to cover all aspects of magnetic structural characterization, but focuses on major modern techniques. Owing to the complexity of magnetic behavior, to tackle one single material problem often necessitates bringing to bear various characterization tools within our arsenal of techniques. Usually, this is not a trivial task. Different research communities employ different research techniques and, often, there is little communication between them. It is my hope that this book will bridge this gap, and make the combined use of various techniques in materials research a reality.

Although this book leans more toward the research laboratory than the classroom, it can serve as a methodological reference book for graduate students, university faculties, scientists and engineers who are interested in magnetic materials and their characterization. Expositions within individual chapters are largely self-contained without having been sequenced with any specific pedagogical thread in mind. Each chapter, therefore, has its own introduction, principle, instrumentation and applications, and references for further study. The level of presentation is intended to be intermediate between a cursory overview and detailed instruction. The extent of coverage is very much dictated by the character of the technique described. Many are based on quite complex concepts and instrumentation. Others are less so, and can be based on commercial products. Researchers working on non-magnetic materials may also find this book useful since many techniques and principles described in the book can be used for characterizing other materials.

Finally, I would like to express my appreciation to the many expert authors who have contributed to this book. On the production side, special thanks go to Lisa Jansson, the type-setting editor at Brookhaven, for her significant role in finalizing the book format, and to my colleague Marco Beleggia, who spent significant amounts of time in helping Lisa on the technical aspects of type-setting, such as the conversion of equations and symbols, and to my student June Lau for checking the Appendices. I am also grateful to the staff at Kluwer Academic Publisher, especially senior editor Greg Franklin, for their help and advice.

Yimei Zhu

Brookhaven National Laboratory
Long Island, New York

Table of Contents

X-ray Scattering

Electron Scattering

Proximal Probe

Light Scattering

Neutron Scattering

CHAPTER 1

Magnetic neutron scattering

1.1. INTRODUCTION

Much of our understanding of the atomic-scale magnetic structure and the dynamical properties of solids and liquids was gained from neutron-scattering studies. Elastic and inelastic neutron spectroscopy provided physicists with an unprecedented, detailed access to spin structures, magnetic-excitation spectra, soft-modes and critical dynamics at magnetic phase transitions, which is unrivaled by other experimental techniques. Because the neutron has no electric charge, it is an ideal weakly interacting and highly penetrating probe of matter's inner structure and dynamics. Unlike techniques using photon electric fields or charged particles (*e.g.*, electrons, muons) that significantly modify the local electronic environment, neutron spectroscopy allows determination of a material's intrinsic, unperturbed physical properties. The method is not sensitive to extraneous charges, electric fields, and the imperfection of surface layers. Because the neutron is a highly penetrating and non-destructive probe, neutron spectroscopy can probe the microscopic properties of bulk materials (not just their surface layers) and study samples embedded in complex environments, such as cryostats, magnets, and pressure cells, which are essential for understanding the physical origins of magnetic phenomena.

Neutron scattering is arguably the most powerful and versatile experimental tool for studying the microscopic properties of the magnetic materials. The magnitude of the cross-section of the neutron magnetic scattering is similar to the cross-section of nuclear scattering by short-range nuclear forces, and is large enough to provide measurable scattering by the ordered magnetic structures and electron spin fluctuations. In the half-a-century or so that has passed since neutron beams with sufficient intensity for scattering applications became available with the advent of the nuclear reactors, they have became indispensable tools for studying a variety of important areas of modern science, ranging from large-scale structures and dynamics of polymers and biological systems, to electronic properties of today's technological materials. Neutron scattering developed into a vast field, encompassing many different experimental techniques aimed at exploring different aspects of matter's atomic structure and dynamics.

Modern magnetic neutron scattering includes several specialized techniques designed for specific studies and/or particular classes of materials. Among these are magnetic reflectometry aimed at investigating surfaces, interfaces, and multilayers, small-angle scattering for the large-scale structures, such as a vortex lattice in a superconductor, and neutron spin-echo spectroscopy for glasses and polymers. Each of these techniques and many others offer exciting opportunities for examining magnetism and warrant extensive reviews, but the aim of this chapter is not to survey how different neutron-scattering methods are used to examine magnetic properties of different materials. Here, we concentrate on reviewing the basics of the magnetic neutron scattering, and on the recent developments in applying one of the oldest methods, the triple axis spectroscopy, that still is among the most extensively used ones. The developments discussed here are new and have not been coherently reviewed. Chapter 2 of this book reviews magnetic small-angle scattering, and modern techniques of neutron magnetic reflectometry are discussed in Chapter 3.

In the first part of this chapter, we give an extensive, coherent introduction to magnetic neutron scattering. It includes an overview of the scattering problem with the derivation of the differential cross-section and its application to the neutron's magnetic interaction with an atom, the evaluation and properties of the magnetic form factors, and, finally, the general properties of the magnetic elastic and inelastic neutron scattering for the spin system of localized atomic electrons in the crystal. We describe magnetic neutron scattering at the "top level", concentrating on the highest-level formulae, but not giving particulars, which can be found in several books [1-5]. Further, rather than being exhaustive, we attempt to summarize those results that are general yet simple, and which, therefore, are most commonly used in everyday research.

The important issue of the magnetic form factors deserves special mention. A very complete theory was developed, accounting quite generally for the spin and the orbital magnetization density of atomic electrons, [3]. However, the general expressions in Ref. [3] are cumbersome so that they are rarely used in practice, and are replaced by the simple, but often highly inaccurate, "dipole approximation". Here, we derive simple formulae for the atomic spin magnetic form factors that accurately account for their angular anisotropy, a tremendous improvement over the dipole approximation. Although these expressions are not as completely general as those of Ref. [3], they accurately describe most situations encountered in magnetic neutron scattering. An example of where using the correct, anisotropic magnetic form factor is crucial for interpreting the experimental results is that of Cu^{2+} spins in topical cuprate materials. This issue gains more importance as magnetic neutron scattering conquers new heights in accessible energy transfers with the development of pulsed spallation neutron sources, such as ISIS in the UK and SNS in the United States. With energy transfers of 0.5 eV and above (see Fig. 1-1 for an example) the measured intensity is collected at very large wave vectors, where the magnetic form factor is small and often pronouncedly anisotropic.

In the second part, we describe the modern uses of the triple-axis spectrometer based on employing a large, multicrystal analyzer and/or the position-sensitive detector (PSD) to analyze the neutrons scattered by the sample. In many instances, the volume of the sample's phase space probed at each spectrometer setting can be increased by about an order-of-magnitude by using the PSD, thereby raising the rate of data collection. These advanced techniques, as known to the authors, were conceived and implemented on SPINS triple axis neutron spectrometer at the NIST Center for Neutron Research (NCNR) in Gaithersburg, MD, United States. Collin Broholm pioneered the PSD setup at the NCNR, with our active participation. It is a natural extension of SPINS capabilities based on employing a large multicrystal analyzer, originally designed for horizontal monochromatic (Rowland) focusing. Reportedly, a similar PSD setup

was implemented on RITA spectrometer at the Risoe National Laboratory, Denmark. However, because the Risoe research reactor was permanently shutdown, the possibilities of RITA were not adequately explored. Subsequently, the spectrometer was moved to SINQ's continuous spallation neutron source at the Paul Sherrer Institute in Switzerland, where it now operates.

While an extensive literature addresses various aspects of neutron-scattering techniques, including several excellent books and monographs on magnetic neutron scattering [1-5], the advances outlined above are recent enough not to be described elsewhere. The general outline of this chapter is as follows. First, we review the fundamentals of neutron scattering: neutron interactions with matter, and magnetic scattering cross-section. We give a detailed exposition on magnetic form factors, deriving some simple and general formulae for the anisotropic form factors of the atomic orbitals that are not readily available elsewhere. Then, we summarize the properties of the two-point magnetization correlation functions in different classes of magnetic materials, paying special attention to pure spin scattering, where we derive the sum rules for the spin correlation function and review the single-mode approximation. Finally, we describe recent advances in triple axis spectroscopy, probably the most powerful technique for studying the dynamical properties of magnetic materials.

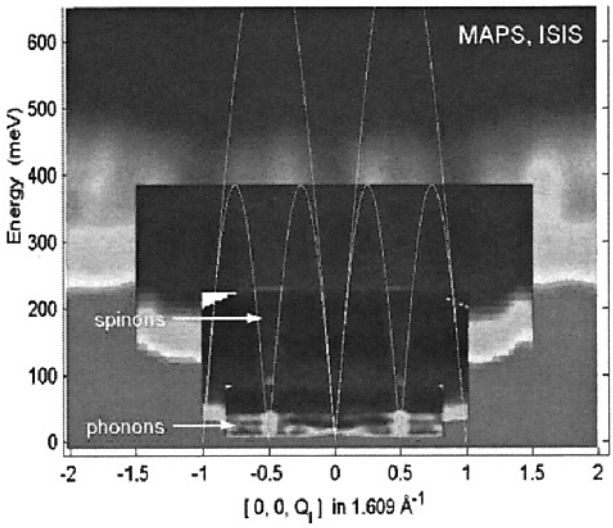

Figure 1-1: Color contour maps of the raw neutron-scattering intensity from a sample of the high-T_c-relative, chain cuprate $SrCuO_2$. The data was collected on MAPS time-of-flight neutron spectrometer at the ISIS pulsed spallation neutron source. Four measurements with the incident neutron energy $E_i \approx 100$, 250, 500 and 850 meV are shown stacked in the figure. They probe the energy transfers up to ≈ 80, 220, 400, and 650 meV, respectively. *Also see the color plate.*

1.2. Neutron interaction with matter and scattering cross-section

In this section, we review some important facts about the neutron, its properties, interaction with matter, and scattering cross-section.

The neutron is one of the basic constituents of matter. Together with its charged relative, the proton, it is a building block of the atomic nuclei (neutrons and protons are fermionic hadrons

that, according to the "standard model", are the baryons, respectively composed of one "up" and two "down" quarks, and two "up" and one "down" quarks). Table 1-1 summarizes the basic properties of a neutron. Although the neutron is electrically neutral, it has a non-zero magnetic moment, similar in magnitude to that of a proton ($\mu_n \approx 0.685\mu_p$), but directed opposite to the angular momentum, so that the neutron's gyromagnetic ratio is negative.

Table 1-1: Basic properties of a neutron (mainly in Gauss CGS units). σ_n denotes the neutron's angular momentum, $\mu_N = e\hbar/(2m_p c) = 5.0508\cdot10^{-24}$ erg/Gs is the nuclear magneton.

Electric charge	Spin $S_n = \sigma_n/\hbar$	Mass m_n (g)	$m_n c^2/e$ (V)	Magnetic moment μ_n (erg/Gs)	Gyromagnetic ratio γ_n, $\boldsymbol{\mu}_n = \gamma_n \boldsymbol{\sigma}_n$ (s^{-1}/Gs)	g-factor g_n, $\boldsymbol{\mu}_n = -g_n \mu_N \boldsymbol{S}_n$	Life-time (s)	Decay reaction
0	1/2	$1.675\cdot10^{-24}$	$0.94\cdot10^{9}$	$9.662\cdot10^{-24}$	$-1.832\cdot10^{4}$	3.826	887	$n \rightarrow p\, e^- \underline{\nu}_e$

Outside the nucleus, a free neutron's lifetime is only about 15 minutes, after which it undergoes a β–decay into a proton, an electron, and an antineutrino. Nevertheless, this lifetime is long enough for neutron-scattering experiments. A neutron extracted through the beam-tube in a nuclear reactor typically has reached thermal equilibrium with the water that cools the reactor in a number of collisions on its way out (such neutrons usually are called thermal neutrons). Assuming the water has "standard" temperature of 293 K, the neutron's most probable velocity would be about 2200 m/s. It would spend only a fraction of a second while it travels in the spectrometer, is scattered by the sample, and arrives in the detector.

Generally, as widely accepted in the neutron-scattering literature, particle-physics notation is followed, and the energies both of a neutron and that of an excitation created in the scattering process are measured in millielectronvolts (meV). To ease comparison with the notations used in other techniques and in theoretical calculations, we list several different ways of representing the neutron's energy, E_n = 1 meV, in Table 1-2. The different energy notations shown in the Table can be used interchangeably, as a matter of convenience.

Table 1-2: Different notations used to represent the neutron's energy. e is the electron charge, h is the Plank's constant, c is the velocity of light, $\mu_B = e\hbar/(2m_e c) = 0.927\cdot10^{-20}$ erg/Gs is the Bohr's magneton, k_B is the Boltzman constant. Also shown are the corresponding neutron wave vector and deBroglie wavelength.

E_n (erg)	E_n/e (meV)	E_n/h (THz)	$E_n/(hc)$ (cm^{-1})	$E_n/(2\mu_B)$ (Gauss)	E_n/k_B (K)	λ_n (Å)	k_n ($Å^{-1}$)
$1.602\cdot10^{-15}$	1	0.2418	8.0655	$8.638\cdot10^{4}$	11.604	9.0437	0.69476

Neutrons used in scattering experiments are non-relativistic. Therefore, the neutron's energy, E_n, is related to its velocity, v_n, wave vector, $k_n = (m_n v_n)/\hbar$, and the (de Broglie) wavelength, $\lambda_n = (2\pi)/k_n$, through

$$E_n = \frac{m_n v_n^2}{2} = \frac{\hbar^2 k_n^2}{2m_n} = \frac{h^2}{2m_n \lambda_n^2}.$$

In a typical experiment, neutrons with energies well in sub-eV range are used, although in some recent ones, the incident neutron energies were as high as 1 eV and more, Fig. 1-1. The

neutron's wavelength and its wave vector are usually measured in Å (1 Å = 0.1 nm = 10^{-8} cm) and $Å^{-1}$, respectively. A useful relation connecting these quantities with the energy in meV follows from Table 2-2,

$$E_n = 2.0717\, k_n^2 = \frac{81.79}{\lambda_n^2}.$$

1.2.1. Basic scattering theory and differential cross-section

The general idea of a (direct geometry) scattering experiment is to place a sample in the beam of incident particles of mass m, with a well-defined wave vector $\boldsymbol{k}_i$ and known incident flux $\Phi_i(\boldsymbol{k}_i)$, and to measure the partial current, $\delta J_f(\boldsymbol{k}_f)$, scattered into a small (≈ infinitesimal) volume of the phase space, $d^3\boldsymbol{k}_f = k_f^2 dk_f d\Omega_f = \left(mk_f/\hbar^2\right) dE_f d\Omega_f$, at a wave vector $\boldsymbol{k}_f$ (Fig.1-2).

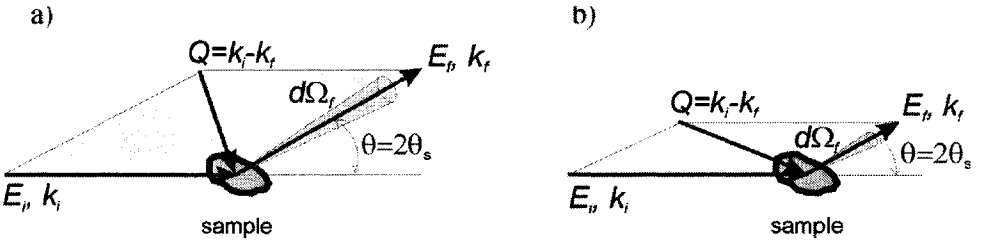

Figure 1-2: Typical geometry of a scattering experiment, (a) elastic, (b) inelastic.

The phase space density of the scattered current, normalized to the incident flux, defines the differential scattering cross-section with respect to the corresponding phase variables. The one most commonly measured and calculated is the double differential scattering cross-section,

$$\frac{d^2\sigma(\boldsymbol{Q},E)}{dEd\Omega} = \frac{1}{\Phi_i(\boldsymbol{k}_i)} \frac{\delta J_f(\boldsymbol{k}_f)}{dE_f d\Omega_f} = \frac{mk_f}{\hbar^2} \frac{1}{\Phi_i(\boldsymbol{k}_i)} \frac{\delta J_f(\boldsymbol{k}_f)}{d^3\boldsymbol{k}_f}. \tag{1.1}$$

Here, the laws of conservation determine the energy, E, and the wave vector, $\boldsymbol{Q}$, transferred to the sample,

$$E = \frac{(\hbar k_i)^2}{2m} - \frac{(\hbar k_f)^2}{2m}, \quad \boldsymbol{Q} = \boldsymbol{k}_i - \boldsymbol{k}_f. \tag{1.2}$$

Lippmann and Schwinger [5,6] most elegantly formulated the general solution of the scattering problem. Let η denote the complete set of variables that describe the state of the scatterer, and let the state of the scattered particle be described by its momentum, $\hbar\boldsymbol{k}$, and its spin quantum number, S^z. The state of the composite system, target sample (scatterer) + scattered particle that satisfies the boundary conditions of the scattering problem and has the energy $E_f^{(tot)} = E_i^{(tot)} = E_i(\eta_i) + (\hbar k_i)^2/(2m)$, is called the scattering state, $\left|\boldsymbol{k}_f, S_f^z, \eta_f\right\rangle$. It is obtained from the initial state, $\left|\boldsymbol{k}_i, S_i^z, \eta_i\right\rangle$, by applying the evolution operator $(1+\mathbf{GT})$,

$$\left|\boldsymbol{k}_f, S_f^z, \eta_f\right\rangle = (1+\mathbf{GT})\left|\boldsymbol{k}_i, S_i^z, \eta_i\right\rangle. \tag{1.3}$$

Here, **T** is the so-called *transition operator*, or *T-matrix*, and **G** is the retarded Green's function,

$$\mathbf{G}^{-1} = \left(E_i^{(tot)} - \mathbf{H}_0 + i \cdot 0\right). \tag{1.4}$$

Here, $\mathbf{H}_0 = \mathbf{H}_s + (\hbar \boldsymbol{k}_i)^2/(2m)$ is the part of the total Hamiltonian, $\mathbf{H} = \mathbf{H}_0 + \mathbf{V}$, which describes the sample and the scattered particle in the absence of their interaction, **V**. The rate of transition, $\Gamma_{i \to f}$, from the initial to the final state ($i \to f$), $\left|\boldsymbol{k}_i, S_i^z, \eta_i\right\rangle \to \left|\boldsymbol{k}_f, S_f^z, \eta_f\right\rangle$, is given by the appropriate matrix element of the transition operator,

$$\Gamma_{i \to f} = \frac{2\pi}{\hbar}\left|\left\langle \boldsymbol{k}_f, S_f^z, \eta_f \left| \mathbf{T} \right| \boldsymbol{k}_i, S_i^z, \eta_i \right\rangle\right|^2 \delta\left(E_i^{(tot)} - E_f^{(tot)}\right) = (2\pi)^3 \frac{\delta J_f(\boldsymbol{k}_f)}{d^3\boldsymbol{k}}. \tag{1.5}$$

It determines the scattered current, $\delta J_f(\boldsymbol{k}_f)$, and, therefore, the scattering cross-section. $E_f^{(tot)} = E_f(\eta_f) + (\hbar k_f)^2/(2m)$ is the energy of the system in the scattered state, so that the energy transfer to the sample is

$$E = E_f(\eta_f) - E_i(\eta_i) = \frac{(\hbar k_i)^2}{2m} - \frac{(\hbar k_f)^2}{2m}, \tag{1.6}$$

as required by the laws of energy conservation, Eq.(1.2). For the initial state of the incident particle in the form of a plane wave normalized to unity probability density, $\langle \boldsymbol{r} | \boldsymbol{k}_i \rangle = e^{i\boldsymbol{k}_i \boldsymbol{r}}$, the incident flux is $\Phi_i(\boldsymbol{k}_i) = \hbar k_i / m$. Substituting this in Eqs.(1.1) and (1.5), the following general expression is straightforwardly obtained for the partial differential scattering cross-section corresponding to the transition $i \to f$,

$$\frac{d^2\sigma(\boldsymbol{Q}, E)}{dE d\Omega} = \frac{k_f}{k_i}\left|\left\langle S_f^z, \eta_f \left| \mathbf{b}(-\boldsymbol{Q}) \right| S_i^z, \eta_i \right\rangle\right|^2 \delta\left(E_i(\eta_i) - E_f(\eta_f) + E\right). \tag{1.7}$$

Here, the numerical pre-factor in front of **T** was conveniently absorbed into the definition of the *scattering length operator* **b**,

$$\mathbf{b} = -\frac{m}{2\pi\hbar^2}\mathbf{T}. \tag{1.8}$$

By definition, $\mathbf{b}(-\boldsymbol{Q}) \equiv \mathbf{b}(-\boldsymbol{Q}, \mathbf{S}, \eta)$ in Eq.(1.7) is the Fourier transform of the matrix element of the scattering length with respect to the coordinate of the scattered particle,

$$\mathbf{b}(\boldsymbol{q}) \equiv \int e^{-i\boldsymbol{q}\boldsymbol{r}'} \left\langle \boldsymbol{r}' \left| \mathbf{b}(\mathbf{r}, \mathbf{S}, \eta) \right| \boldsymbol{r}' \right\rangle d^3\boldsymbol{r}' = \left\langle \boldsymbol{k}_f \left| \mathbf{b}(\mathbf{r}, \mathbf{S}, \eta) \right| \boldsymbol{k}_i \right\rangle, \tag{1.9}$$

for the wave vector $\boldsymbol{q} = \boldsymbol{k}_f - \boldsymbol{k}_i = -\boldsymbol{Q}$ that is transferred to that particle.

Finally, the **T**-matrix operator satisfies the Lippmann-Schwinger equation, $\mathbf{T} = \mathbf{V} + \mathbf{TGV}$. Its iterative solution can be found in the form of the Born perturbation series (more generally, the von Neumann series) [5],

$$\mathbf{T} = \mathbf{V} + \mathbf{VGV} + \mathbf{VGVGV} + \ldots = \mathbf{V}\left(1 + \sum_n (\mathbf{GV})^n\right), \tag{1.10}$$

that completes the general solution of the scattering problem (provided the perturbation series converge). In many important cases, it appears sufficient to retain only the first-order term in

this expansion, and use

$$\mathbf{T} = \mathbf{V}, \quad \mathbf{b} = -\frac{m}{2\pi\hbar^2}\mathbf{V}, \tag{1.11}$$

that is known as the *Born approximation*. An expression for the transition rate in this approximation, obtained by substituting **T**=**V** into Eq.(1.8) is one of the cornerstone results of Quantum Mechanics [7,8], and is universally used to describe scattering processes. Following Fermi, this expression often is called the "golden rule" [1,4].

1.2.2. Neutron interactions and scattering lengths

Two fundamental interactions govern the scattering of neutrons by an atomic system and define the neutron scattering cross-section measured in an experiment. The residual strong interaction, also known as the nuclear force, gives rise to scattering by the atomic nuclei (nuclear scattering). The electromagnetic interaction of the neutron's magnetic moment with the sample's internal magnetic fields gives rise to magnetic scattering. The sample's internal magnetic fields mainly originate from unpaired electrons in the atomic shells.

1.2.2.1. Nuclear scattering length

While magnetic interaction is relativistic and extremely weak, the nuclear force is not (as it is responsible for holding together protons and neutrons in the nucleus). However, it has extremely short range, 10^{-13} cm to 10^{-12} cm, comparable with the size of the nuclei, and much smaller than the typical neutron's wavelength. Consequently, away from the conditions of the resonance neutron capture, the probability of a neutron being scattered by an individual nucleus is very small, and can be treated in the scattering theory on par with the probability of magnetic scattering. In fact, it appears that nuclear scattering length, b_N, for the majority of natural elements is close in magnitude to the characteristic magnetic scattering length, $r_m = -(g_n/2)r_e = -5.391$ fm (1 fm = 10^{-13} cm, $r_e = e^2/(m_e c^2)$ is the classical electron radius).

To describe the neutron's interaction with the atomic system in which the typical distances are about 1 Å, the nuclear scattering length operator can be effectively treated as a delta-function in the coordinate representation,

$$\mathbf{b}_N = b_N \delta(\boldsymbol{r}_n - \boldsymbol{R}), \tag{1.12}$$

where $\boldsymbol{r}_n$ is a coordinate of a neutron and $\boldsymbol{R}$ is that of a nucleus. Alternatively, in the momentum representation it is just a number (for the nucleus fixed at the origin), $\mathbf{b}_N(\boldsymbol{q}) = b_N$, independent of the incident neutron's wave-vector and of the wave-vector transfer, $\boldsymbol{q}$. This again indicates that the applicability of such treatment is limited to neutrons whose wavelength is large enough compared to the size of the nuclei. In the Born approximation, Eq.(1.12) for the scattering length would correspond to the neutron-nucleus interaction,

$$\mathbf{V}_N(\boldsymbol{r}_n, \boldsymbol{R}) = -\frac{2\pi\hbar^2}{m_n} b_N \delta(\boldsymbol{r}_n - \boldsymbol{R}), \tag{1.13}$$

generally known as the Fermi pseudopotential [1,9]. In Eqs.(1.12) and (1.13), the scattering length refers to the fixed nucleus and is called the bound scattering length. Usually, it is treated

as a phenomenological parameter that is determined experimentally [10]. In general, the bound scattering length is considered to be a complex quantity, $b_N = b' - ib''$, defining the total scattering cross-section, σ_s, and the absorption cross-section far from the nuclear resonance capture, σ_a, through

$$\sigma_s = 4\pi|b|^2, \quad \sigma_a = \frac{4\pi}{k_i} b''. \tag{1.14}$$

Ref. [11] tabulates the bound scattering lengths and cross sections of the different elements and their isotopes.

1.2.2.2. Magnetic scattering length

Because the magnetic interaction of a neutron with a single atom is very weak, the Born approximation, Eq.(1.11), very accurately describes the magnetic scattering length. The main contribution to magnetic scattering arises from the neutron's interaction with the total dipole magnetic moment of the atomic electrons; all other electromagnetic interactions are at least two orders-of-magnitude smaller and can be safely neglected [5]. The fundamental starting point for evaluating the neutron magnetic scattering length is the Hamiltonian of the electrons in the atom in the presence of the neutron's magnetic field [2,4]. The interaction Hamiltonian is

$$\mathbf{V}_m(\boldsymbol{r}_n, \boldsymbol{r}_e) = \sum_e \left\{ \frac{2\mu_B}{\hbar} (\boldsymbol{A}_n(\boldsymbol{r}_e) \cdot \boldsymbol{p}_e) + 2\mu_B (\boldsymbol{s}_e \cdot \boldsymbol{H}_n(\boldsymbol{r}_e)) \right\} = \sum_e \{\mathbf{V}_{le} + \mathbf{V}_{se}\}, \tag{1.15}$$

where the sum extends over all electrons in the atom, indexed by e. $\boldsymbol{r}_n$ and $\boldsymbol{r}_e$ are the position of the neutron and that of the electron, respectively, $\boldsymbol{p}_e$ is the momentum, and $\hbar\boldsymbol{s}_e$ is the spin angular momentum of the electron. $\boldsymbol{A}_n(\boldsymbol{r}_e)$ is the vector-potential, so that

$$\boldsymbol{H}_n(\boldsymbol{r}_e) = [\nabla_{\boldsymbol{r}_e} \times \boldsymbol{A}_n(\boldsymbol{r}_e)] \tag{1.16}$$

is the magnetic field of the neutron at the position of the e^{th} electron, $\boldsymbol{r}_e$. The first term in Eq.(1.15), $\mathbf{V}_{le}$, describes the interaction of the neutron magnetic field, $\boldsymbol{H}_n(\boldsymbol{r}_e)$, with the electric current produced by the electron's orbital motion. The second term, $\mathbf{V}_{se}$, accounts for the neutron's magnetic interaction with the spin magnetic moment of the electrons.

The characteristic size of the inner structure of a neutron is extremely small, so that in describing the magnetic interaction with an electron in an atom it can be treated as a point dipole with the magnetic moment $\boldsymbol{\mu}_n = \gamma_n \boldsymbol{\sigma}_n$, γ_n is the neutron's gyromagnetic ratio, and $\boldsymbol{\sigma}_n = \hbar\boldsymbol{s}_n$ is its spin angular momentum (see Table 1-1). The corresponding expression for the neutron's magnetic field vector potential at the position of the electron is

$$\boldsymbol{A}_n(\boldsymbol{r}_e) = \left[\boldsymbol{\mu}_n \times \frac{\boldsymbol{r}_e - \boldsymbol{r}_n}{|\boldsymbol{r}_e - \boldsymbol{r}_n|^3} \right] = \left[\nabla_{\boldsymbol{r}_e} \times \frac{\boldsymbol{\mu}_n}{|\boldsymbol{r}_e - \boldsymbol{r}_n|} \right] = \left[\nabla \times \frac{\boldsymbol{\mu}_n}{r} \right], \tag{1.17}$$

$\boldsymbol{r} = \boldsymbol{r}_e - \boldsymbol{r}_n$ is the spacing between the neutron and the electron [2,3-5,12].

On account of Eq.(1.17), the orbital part of the interaction Hamiltonian Eq.(1.15) can be recast in the following form,

$$\mathbf{V}_{le} = -\left(\boldsymbol{\mu}_n \cdot \left[\nabla \times \left(\frac{1}{r}\frac{e}{m_e c}\boldsymbol{p}_e\right)\right]\right) = 2\mu_B \frac{(\boldsymbol{\mu}_n \cdot \boldsymbol{l}_e)}{r^3}, \tag{1.18}$$

which also could be semirigorously derived from the Biot-Savart law [1,12]. Here $\boldsymbol{p}_e$ is the momentum of the electron, and $\hbar \boldsymbol{l}_e = [\boldsymbol{r} \times \boldsymbol{p}_e]$ is its orbital angular momentum in the neutron's rest frame. Eq.(1.18) is just the energy of the neutron's dipole magnetic moment, $\boldsymbol{\mu}_n$, in the magnetic field,

$$\boldsymbol{H}_{le}(\boldsymbol{r}_n) = \left[\frac{(\boldsymbol{r}_e - \boldsymbol{r}_n)}{|\boldsymbol{r}_e - \boldsymbol{r}_n|^3} \times \frac{1}{c}\boldsymbol{I}_e\right] = \left[\nabla_{\boldsymbol{r}_n}\left(\frac{1}{r}\right) \times \frac{1}{c}\boldsymbol{I}_e\right] = \left[\nabla \times \left(-\frac{1}{cr}\boldsymbol{I}_e\right)\right], \tag{1.19}$$

of the electron's orbital electric current $\boldsymbol{I}_e$, [12]. The latter is formally defined by $\boldsymbol{I}_e = -(e/m_e)\boldsymbol{p}_e$ [note, that $\nabla_{\boldsymbol{r}_e} f(r) = \nabla f(r) = -\nabla_{\boldsymbol{r}_n} f(r)$].

The second term in Eq.(1.15), describing the neutron's interaction with the spin magnetic moment of the electron, $\boldsymbol{\mu}_{se} = -2\mu_B \boldsymbol{s}_e$, can be rewritten symmetrically as the interaction of the two magnetic point dipoles at a distance $r = |\boldsymbol{r}_e - \boldsymbol{r}_n|$ from each other,

$$\mathbf{V}_{se}(\boldsymbol{r}) = -\left(\boldsymbol{\mu}_{se} \cdot \left[\nabla \times \left[\nabla \times \frac{\boldsymbol{\mu}_n}{r}\right]\right]\right) = -\left(\boldsymbol{\mu}_n \cdot \left[\nabla \times \left[\nabla \times \frac{\boldsymbol{\mu}_{se}}{r}\right]\right]\right). \tag{1.20}$$

This expression contains essential singularity at $\boldsymbol{r} = 0$ and needs to be treated carefully when evaluating the derivatives. By using $\nabla^2(1/r) = -4\pi\delta(\boldsymbol{r})$, Eq.(1.20) can readily be transformed to the form perhaps most commonly used for the interaction between two point dipoles [13-15],

$$\mathbf{V}_{se}(\boldsymbol{r}) = -\left\{\frac{8\pi}{3}(\boldsymbol{\mu}_n \cdot \boldsymbol{\mu}_{se})\delta(\boldsymbol{r}) - \frac{(\boldsymbol{\mu}_n \cdot \boldsymbol{\mu}_{se})}{r^3} + \frac{3(\boldsymbol{\mu}_n \cdot \boldsymbol{r})(\boldsymbol{\mu}_{se} \cdot \boldsymbol{r})}{r^5}\right\}. \tag{1.21}$$

The first, singular term here is called the Fermi contact interaction. The rest is the potential part that describes the interaction between the dipoles at large distances. Because the neutron's wave function overlaps with those of the electrons, it is essential to account for the contact term in the magnetic scattering length. Although less conventional, Eq.(1.20) is more convenient for evaluating the scattering cross-section. Not only does it correctly contain the singular part of the dipole-dipole interaction, but it also can be readily Fourier-transformed to obtain the spin contribution to the neutron's magnetic scattering length in the momentum representation

$$\mathbf{b}_{se}(\boldsymbol{q}) = \int e^{-i\boldsymbol{q}\boldsymbol{r}_n} \mathbf{b}_{se}(\boldsymbol{r}_n, \boldsymbol{r}_e) d^3 r_n = -\frac{m}{2\pi\hbar^2}\frac{4\pi}{q^2}\left(\boldsymbol{\mu}_n \cdot \left[\boldsymbol{q} \times \left[\boldsymbol{q} \times e^{-i\boldsymbol{q}\boldsymbol{r}_e}\boldsymbol{\mu}_{se}\right]\right]\right). \tag{1.22}$$

This expression is an important, fundamental result that governs the essential properties of the magnetic neutron scattering cross-section.

In many important cases, the contribution of the orbital currents to the magnetic scattering cross-section Eq.(1.7) is zero, or small, and can be neglected. This happens when the corresponding matrix elements of the orbital contribution Eq.(1.18) to the magnetic interaction are small, or vanish, as is the case, for example, for scattering by the *s*-electrons that are in the $l_e = 0$ state and, consequently, $\langle \eta_f | \mathbf{V}_{le} | \eta_i \rangle = 0$. For atoms of the transition elements in the crystal, the local crystal electric field typically quenches orbital angular momentum [14]. Hence, the orbital contribution to the magnetic scattering cross-section also is very small. On the other hand,

accurately accounting for the orbital scattering is rather cumbersome, much more so than for spin-only scattering. This is because the matrix elements of the orbital part of the magnetic interaction, Eq.(1.18), depend significantly on the electron's wave functions and, in general, require specific calculations for each particular case of electronic configuration in the atom [17-22]. On these grounds, the orbital contribution is often discarded in the textbook treatments of the magnetic neutron scattering cross-section, [2,5,15].

Accounting for the orbital magnetic moment is important for the scattering by the 4*f*- and 5*f*-electrons in the rare earths. In this case, the crystal field is usually well screened by the filled outer atomic shells, and the total angular momentum, $\boldsymbol{J} = \boldsymbol{L} + \boldsymbol{S}$, is a good quantum number. Fortunately, the useful general expressions for the magnetic neutron scattering length and for the corresponding cross-section can be derived without first evaluating the matrix elements of the orbital part of the neutron's magnetic interaction with the electrons. This task can be postponed till the end, where it becomes a part of the general problem of evaluating the atom's magnetic form factor.

One proceeds as follows. Under very general assumptions, the orbital contribution to the magnetic neutron-scattering length can be transformed to a form similar to the spin part, Eqs. (1.20) and (1.22). Consequently, they can be combined and treated together. The simplest way to do this is to assume that the main contribution to the matrix elements of the interaction of the neutron in the plane-wave state with the orbital electron current, Eq.(1.18), comes from the region $r_n >> r_e$. This approximation clearly holds if the neutron's wavelength is much greater than the characteristic size of the atomic wave functions, *i.e.,* for slow neutrons. Then, $1/|\boldsymbol{r}_n - \boldsymbol{r}_e|$ can be expanded in the power series and, to the leading order, the matrix element of the orbital magnetic field at the neutron's position becomes [12]

$$\langle \eta_f | \boldsymbol{H}_{le}(\boldsymbol{r}_n) | \eta_i \rangle = -\frac{2\mu_B}{\hbar} \langle \eta_f | \left[\nabla_{r_n} \times \left(1 - (\boldsymbol{r}_e \cdot \nabla_{r_n})\right) \frac{1}{r_n} \boldsymbol{p}_e \right] | \eta_i \rangle . \tag{1.23}$$

The first term in the inner brackets here does not contribute to the result because, for an electron that remains localized on an atomic orbital, the average momentum is zero, $\langle \eta_f | \boldsymbol{p}_e | \eta_i \rangle = 0$, [12,13]. The second term can be transformed by separating the full time derivative, whose matrix element for an electron in a stationary state is also zero, and using $m_e \dot{\boldsymbol{r}}_e = \boldsymbol{p}_e$, [13],

$$(\boldsymbol{r}_e \cdot \nabla_{r_n}) \boldsymbol{p}_e = \frac{1}{2} \left\{ m_e \frac{d}{dt} \left((\boldsymbol{r}_e \cdot \nabla_{r_n}) \boldsymbol{r}_e \right) - \boldsymbol{r}_e (\boldsymbol{p}_e \cdot \nabla_{r_n}) + (\boldsymbol{r}_e \cdot \nabla_{r_n}) \boldsymbol{p}_e \right\} . \tag{1.24}$$

It then follows that,

$$\langle \eta_f | (\boldsymbol{r}_e \cdot \nabla_{r_n}) \boldsymbol{p}_e | \eta_i \rangle = -\langle \eta_f | [\nabla_{r_n} \times [\boldsymbol{r}_e \times \boldsymbol{p}_e]] | \eta_i \rangle ,$$

and, as a result, Eq.(1.23) becomes

$$\langle \eta_f | \boldsymbol{H}_{le}(\boldsymbol{r}_n) | \eta_i \rangle = -\mu_B \langle \eta_f | \left[\nabla_{r_n} \times \left[\nabla_{r_n} \times \frac{1}{r_n} \boldsymbol{l}_e \right] \right] | \eta_i \rangle . \tag{1.25}$$

This brings the matrix element of the orbital part of the magnetic interaction to the same form as that for the spin part, Eq.(1.20), but with r_n in place of r and with the orbital magnetic moment,

$$\boldsymbol{\mu}_{le} = -\frac{\mu_B}{\hbar} [\boldsymbol{r}_e \times \boldsymbol{p}_e] = -\mu_B \boldsymbol{l}_e , \tag{1.26}$$

replacing the spin magnetic moment, $\boldsymbol{\mu}_{se} = -2\mu_B \boldsymbol{s}_e$.

Both contributions can be combined into a simple final expression for the matrix element of the atom's magnetic neutron scattering length,

$$\langle \boldsymbol{k}_f, \eta_f | \mathbf{b}_m | \boldsymbol{k}_i, \eta_i \rangle = -\frac{m}{2\pi\hbar^2}\frac{4\pi}{q^2}\left(\boldsymbol{\mu}_n \cdot \left[\boldsymbol{q}\times\left[\boldsymbol{q}\times\langle \eta_f | \boldsymbol{M}(\boldsymbol{q}) | \eta_i \rangle\right]\right]\right), \tag{1.27}$$

where $\boldsymbol{q} = \boldsymbol{k}_f - \boldsymbol{k}_i$ is the neutron's wave vector change, as in Eq.(1.9). The approximation adopted above in deriving the Eq.(1.25) gives only the lowest-order, $\boldsymbol{q}$-independent orbital contribution to the operator $\boldsymbol{M}(\boldsymbol{q})$. In this approximation $\boldsymbol{M}(\boldsymbol{q}) \approx \boldsymbol{M}(0) = -\mu_B \sum_e \{\boldsymbol{l}_e + 2\boldsymbol{s}_e\} = -\mu_B(\boldsymbol{L} + 2\boldsymbol{S})$ [16]. Trammel [17] developed a more accurate accounting for the orbital part of the magnetic interaction. His treatment is essentially similar to the above, but the terms of all orders are consistently retained in the series expansion. Consequently, $\boldsymbol{M}(\boldsymbol{q})$ in the right-hand side of Eq.(1.27) becomes

$$\boldsymbol{M}(\boldsymbol{q}) = \sum_e \left\{ -2\mu_B \boldsymbol{s}_e e^{-i\boldsymbol{q}\boldsymbol{r}_e} - \mu_B \frac{1}{2}\left(\boldsymbol{l}_e f(\boldsymbol{q}\cdot\boldsymbol{r}_e) + f(\boldsymbol{q}\cdot\boldsymbol{r}_e)\boldsymbol{l}_e\right)\right\}, \tag{1.28}$$

where

$$f(\boldsymbol{q}\cdot\boldsymbol{r}_e) = 2\sum_{n=0}^{\infty} \frac{(i\boldsymbol{q}\cdot\boldsymbol{r}_e)^n}{n!(n+2)}. \tag{1.29}$$

Eq.(1.25) retains only the first, zero-order, ~$O(q^0)$, term in this expression.

Clearly, the first term in Eq.(1.28) is simply the Fourier-transform of the density of the spin magnetic moment of the atomic electrons

$$\boldsymbol{M}_S(\boldsymbol{q}) = -2\mu_B \sum_e \int e^{-i\boldsymbol{q}\boldsymbol{r}_e} \boldsymbol{s}_e \delta(\boldsymbol{r}' - \boldsymbol{r}_e) d^3\boldsymbol{r}' = \int e^{-i\boldsymbol{q}\boldsymbol{r}'} (-2\mu_B \boldsymbol{S}(\boldsymbol{r}')) d^3\boldsymbol{r}'. \tag{1.30}$$

It also can be shown, [18,19], that the second (orbital) term in Eq.(1.28) is the Fourier-transform of the atom's orbital magnetization density

$$\boldsymbol{M}_L(\boldsymbol{q}) = \sum_e \int e^{-i\boldsymbol{q}\boldsymbol{r}'} \boldsymbol{\mu}_{el}(\boldsymbol{r}') d^3\boldsymbol{r}'. \tag{1.31}$$

Here, the density of the orbital magnetization for an electron in the atom, $\boldsymbol{\mu}_{el}(\boldsymbol{r})$, is defined by the relation $\boldsymbol{j}_e(\boldsymbol{r}) = c[\nabla \times \boldsymbol{\mu}_{el}(\boldsymbol{r})]$, so that it determines the density of the orbital electric current

$$\boldsymbol{j}_e(\boldsymbol{r}) = -\frac{e}{2m_e}\{\boldsymbol{p}_e \delta(\boldsymbol{r} - \boldsymbol{r}_e) + \delta(\boldsymbol{r} - \boldsymbol{r}_e)\boldsymbol{p}_e\} = c[\nabla \times \boldsymbol{\mu}_{el}(\boldsymbol{r})], \tag{1.32}$$

and accounts for the magnetic field arising from the electron's orbital motion. Consequently, the contribution of the orbital electric currents to the magnetic interaction in Eq.(1.15) can be recast in the form of the double cross product, as in Eq.(1.27), using

$$e^{-i\boldsymbol{q}\boldsymbol{r}_e}\frac{1}{c}\boldsymbol{I}_e = \int e^{-i\boldsymbol{q}\boldsymbol{r}'}\frac{1}{c}\boldsymbol{j}_e(\boldsymbol{r}')d^3\boldsymbol{r}' = \int e^{-i\boldsymbol{q}\boldsymbol{r}'}[\nabla_{\boldsymbol{r}'} \times \boldsymbol{\mu}_{el}(\boldsymbol{r}')]d^3\boldsymbol{r}'. \tag{1.33}$$

Therefore, the matrix element of the neutron magnetic scattering length is expressed by the Eq.(1.27), where $\boldsymbol{M}(\boldsymbol{q})$ *is the Fourier-transform of the total*, spin and orbital, *electronic magnetization density in the atom*,

$$\boldsymbol{M}(\boldsymbol{q}) = \boldsymbol{M}_S(\boldsymbol{q}) + \boldsymbol{M}_L(\boldsymbol{q}) = \int e^{-i\boldsymbol{q}\boldsymbol{r}'} \sum_e \{-2\mu_B \boldsymbol{s}_e \delta(\boldsymbol{r}' - \boldsymbol{r}_e) + \boldsymbol{\mu}_{el}(\boldsymbol{r}')\} d^3\boldsymbol{r}'. \tag{1.34}$$

1.2.3. Factorization of the magnetic scattering length and the magnetic form factors

By applying the Wigner-Eckart theorem, a matrix element of the atom's magnetization density operator Eq.(1.34) can be factorized into the product of the reduced matrix element that does not depend on the direction of the atom's angular momentum, and the Wigner 3*j*-symbol, which entirely accounts for such dependence [8,13]. The first factor contains the $\boldsymbol{q}$-dependence of the matrix element, while the second describes its symmetry with respect to rotations and relates them to the magnetic neutron scattering cross-section. Such factorization is extremely useful in understanding magnetic neutron scattering by macroscopic samples. It splits the task of calculating the scattering cross-section for a system of many atoms in two separate major parts that address different aspects of the problem. One is that of evaluating the neutron magnetic form factor, which describes the $\boldsymbol{q}$-dependence of the scattering by a single atom and is determined by the reduced matrix element(s). The other one is that of properly adding the contributions from the correlated (and/or the uncorrelated) rotations of the magnetic moments of different atoms in the sample to obtain the total scattering cross-section.

Because $\boldsymbol{M}(\boldsymbol{q})$ in Eq.(1.27) contains both spin and orbital contributions [*cf* Eq.(1.34)], its matrix elements must be expressed through those of the atom's *total* angular momentum, $\boldsymbol{J}=\boldsymbol{L}+\boldsymbol{S}=\sum_e \{\boldsymbol{l}_e+\boldsymbol{s}_e\}$. Consequently, the Wigner-Eckart theorem applies directly to $\langle \eta_f | \boldsymbol{M}(\boldsymbol{q}) | \eta_i \rangle$ only if $|\eta_i\rangle$ and $|\eta_f\rangle$ are approximately the eigenstates of J and J^z, *i.e.*, if $\boldsymbol{J}$ is an integral of motion for the scattering atom. In practice, this is the case if the spin-orbit interaction (*LS*-coupling) is much larger than any other interaction that depends on the atom's orbital and/or spin angular momentum, such as the interaction with the crystal field. We consider such a situation first.

From Eq.(1.28) we see that the matrix elements of the operators $\boldsymbol{M}_S(\boldsymbol{q})$ and $\boldsymbol{M}_L(\boldsymbol{q})$ between the eigenstates of the atom's total angular momentum, $\boldsymbol{J}$, satisfy the "dipole" selection rules, [7,8]. Hence, for each of the two operators only the matrix elements between the states with $\Delta J = J(\eta_f) - J(\eta_i) = 0, \pm 1$ can differ from zero. Therefore, only such transitions are allowed in the magnetic neutron scattering. This also is evident from the conservation of the total, neutron's and atom's angular momentum, since ΔJ^z has to be offset by the change in the neutron's spin, which can only be $\Delta S_n^z = 0, \pm 1$.

While the Wigner-Eckart decomposition of the matrix element is quite tedious for a general tensor and for an arbitrary states $|\eta_i\rangle$ and $|\eta_f\rangle$, it is greatly simplified for a vector operator such as $\boldsymbol{M}(\boldsymbol{q})$ that is a tensor of rank one [3,13]. As discussed above, the matrix elements of a vector satisfy the "dipole" selection rules, *i.e.*, they can only be non-zero between the states whose angular momentum quantum numbers differ by no more than 1 [13]. Therefore, no more than three different reduced matrix elements appear in the decomposition of $\langle \eta_f | \boldsymbol{M}(\boldsymbol{q}) | \eta_i \rangle$ in Eq.(1.27) and, consequently, in the magnetic neutron scattering cross-section. These reduced matrix elements completely account for the $\boldsymbol{q}$-dependence of magnetic neutron scattering from a single atom. Normalized to 1 at $\boldsymbol{q} = 0$, they define the atom's neutron magnetic form factors for the corresponding scattering channels, in complete analogy with the usual x-ray atomic form factors.

In most cases of practical importance for magnetic neutron scattering, both the initial and the final states of the atom, $|\eta_i\rangle$ and $|\eta_f\rangle$, belong to the *same* angular momentum multiplet, $|\eta_{i,f}\rangle = |\eta', J, J^z_{i,f}\rangle$. There are no transitions between atomic states with different angular momenta, *i.e.*, $J(\eta_f) - J(\eta_i) = 0$. Hence, the cross-section involves only a single reduced matrix element, that for the ground-state multiplet. Normalized appropriately, it defines what is